https://doi.org/10.2352/EI.2026.38.6.ISS-292


# Nano-light pillar structure applied on 1.6 μm pixel size of CMOS image sensor for high sensitivity

*Chun-Yuan Wang, Chung-Hsuan Yu, Ken Chou, Yu-Shen Lu, Hao-Wei Liu, Jian Wen Luo, Shin-Hong Kuo, Yuchi Chang, Huang-Jen Chen, Po-Hsiang Wang, Peter Chiu, JB. Lin and Chin-Chuan Hsieh*

**VisEra Technologies Company, No12, Dusing Rd.1, Hsinchu Science Park, Taiwan (30078)**

**Email: Robert_Wang@viseratech.com**

## Abstract:

*We demonstrated a die-level CMOS image sensor featuring 1.6 μm pixels and integrated nano-light pillars. This design achieved a 1.5 dB improvement in the signal-to-noise ratio (SNR). With an optimal pillar arrangement, the efficiency ratio between the die center and ide edge is comparable to conventional image sensors, while maintaining an acceptable Gr-Gb signal difference.*

## Introduction

Sensitivity has always been a critical factor in CMOS image sensors (CIS). Regardless of the generation, a CIS with high sensitivity offers broader applicability and is less constrained by variations in user environments. However, the sensitivity of conventional CMOS image sensors is fundamentally constrained by pixel size. Traditional CIS designs employ a microlens (ML) as the primary light-receiving structure, and its physical dimensions inherently limit the effective light-collection area. Consequently, the total light flux incident on the pixel is directly proportional to the final signal-to-noise ratio (SNR) of the image sensor. Over the past five years, artificial metasurfaces [1–2] have emerged as potential replacements for conventional microlenses, enabling precise control of light propagation [3] or serving as color-routing elements to overcome the physical limitations of the light-receiving area and enhance sensitivity [4–7], particularly for small-pixel applications.

However, in automotive applications, relatively large-pixel sensors are still commonly used, typically with pixel sizes greater than 1 μm. High sensitivity remains a crucial requirement for autonomous driving. Therefore, integrating large-pixel sensors with metasurfaces for sensitivity enhancement continues to attract significant attention. In this work, we demonstrate a double-layer nano-light pillar (NLP) design implemented on a 1.6 μm pixel image sensor (Fig.1), achieving a 1.5 dB improvement in sensitivity. Furthermore, we employ an organic material for the NLP, offering advantages in cost-effectiveness and stress compatibility for sensor integration.

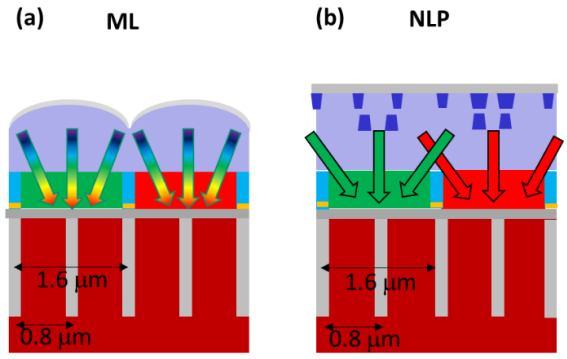


**Fig. 1.** Schematic diagram of ML-CIS and NLP-CIS. (**a**) Congenital ML type of image sensor (**b**). NLP type image sensor. It applied on 0.8 um pixel size with 4-cell binning mode.

### Design concept

To achieve effective color routing on a 1.6 μm pixel, precise control of light propagation toward the target position is required. Due to the spectral overlap among different color channels, it is challenging to achieve clean separation of the RGB components. Therefore, more complex structural patterns are often necessary to manipulate the light distribution accurately. For instance, a three-dimensional electromagnetic (EM) inverse design approach can generate freeform patterns that potentially provide an optimal solution [8]. However, the realization of such complex freeform structures is constrained by lithographic limitations. A simpler and more practical approach involves employing circular-shaped pillars with specially arranged geometries to control phase matching and light scattering. By tuning the pillar size and their

corresponding position to achieve phase matching, the incident light can be focused precisely onto the desired location, including from die-center to high chief ray angle (CRA).

### Fabrication of NLPs

In this work, to realize the 1.6 µm-pixel CMOS image sensor, a 0.8 µm pixel design operated in a four-cell binning mode was adopted as the test vehicle. A double-layer NLP configuration was fabricated on a 1.6 µm Bayer-pattern image sensor. The bottom layer consists of pillar type structures, while the top layer features hole type patterns. The NLP material is a polymer-based composite containing $TiO_2$ nanoparticles, with a refractive index that depends on the $TiO_2$ density, typically ranging from 1.7 to 2.1.

All NLPs were fabricated using standard semiconductor processes, including spin coating, lithography, and etching. In particular, the lithographic patterning was performed using deep ultraviolet (DUV) exposure with a krypton fluoride (KrF) source, providing a cost-effective solution. A transparent separation layer with a refractive index lower than that of the NLPs was inserted between the NLPs and the color filter. A cross-sectional transmission electron microscopy (TEM) image of the fabricated structure is shown in Fig. 2.

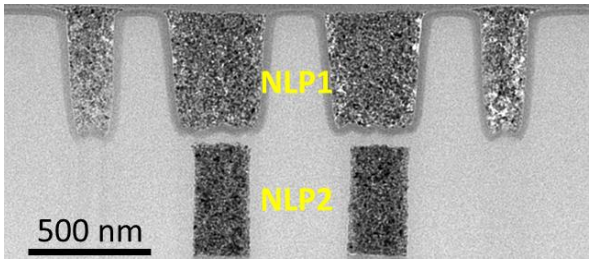


**Fig. 2.** The TEM image of NLP structure.

### Experimental result and discussion

Figures 3–8 illustrate the imaging characteristics of the 1.6 µm-pixel image sensor. First, the quantum efficiency (QE) spectra were measured under normally incident plane waves at individual wavelengths (Fig. 3). The image sensor integrated with NLPs exhibits a higher QE peak compared to the conventional ML type. The peak QE values for the red, green, and blue channels are enhanced by approximately 5%, 11%, and 19%, respectively. However, the NLPs show slightly higher optical crosstalk at 530 nm in the red channel, which may be attributed to light scattering induced by the backside deep trench isolation (BDTI) structure. In principle, this 530 nm crosstalk can be mitigated in an actual single-cell 1.6 µm pixel design. Based on the QE spectra, the SNR10 of the NLP device remains superior to that of the ML type, with an overall improvement of approximately 19%.

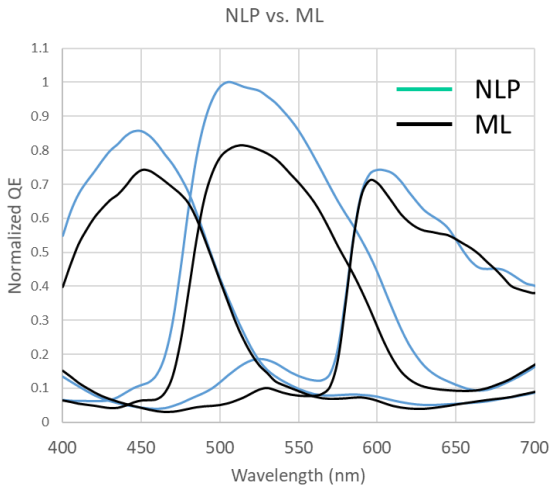


**Fig. 3.** The QE spectrum of NLP type sensor and ML type sensor. The blue solid lines show QE spectrum of NLP type sensor. The black solid lines show the QE spectrum of ML type sensor.

Second, Fig. 4 presents the white-screen image of the full sensor die, captured through a module lens with a F-number of 2.0. The maximum CRA of this lens is 29° at 100% image height. From the white-screen image, the angular response behavior of the NLP device as a function of image height closely resembles that of the ML device, indicating that optical efficiency at larger image heights can also be effectively maintained by the NLP design. This performance is attributed to the optimized pillar positioning at the die edge, which compensates for the increased CRA.

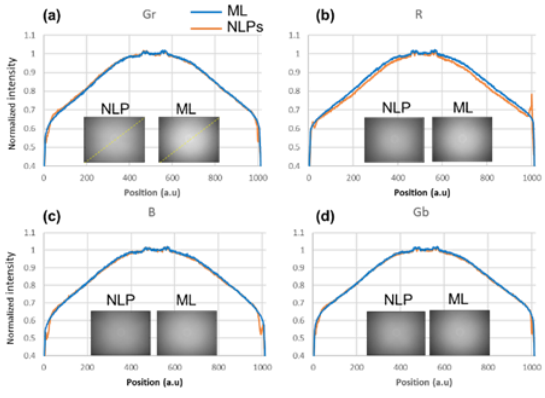


**Fig. 4.** Light shading behavior of image sensor with module lens of F/#2.0. The normalized light intensity curve of light shading curve for each channel: (a) Gr binning channels. (b) R binning channels (c) B binning channels. (d) Gb binning channels. The light shading curve are plot along the yellow dash line of white screen picture. The maximum image height is at CRA=29 degree

Third, Fig. 5 shows the mapping of the Gr-Gb difference across the full die. The maximum Gr-Gb variation is approximately 2.3%, which is comparable to previously literature results [3,7] but is slight higher than conventional ML sensor (usually < 2%) . The slight asymmetry in the Gr-Gb difference is mainly due to manual alignment errors between module lens and image sensor during module lens assembly.

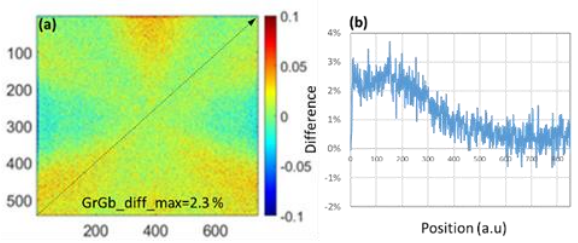


**Fig. 5.** The channel difference mapping of Gr and Gb binning mode. (**a**) GrGb channel difference mapping. (**b**) the GrGb difference plots from the black dash line from **fig. 5a**.

The full-die color images are shown in Fig. 6. Two illumination conditions were evaluated to compare imaging performance. Under the high-illumination condition (500 lux), according to the color chart results and subsequent image signal processing, the SNR of the NLP type sensor improved by approximately 1.5 dB. The color error (ΔE = 3.33) of the NLP device remained comparable to that of the ML type sensor (ΔE = 3.24). Under the low-illumination condition (20 lux), similar behavior was observed. The SNR of the NLP device improved by about 1.3 dB, while the color error remained at a similar level compared with the ML type sensor (Fig. 7).

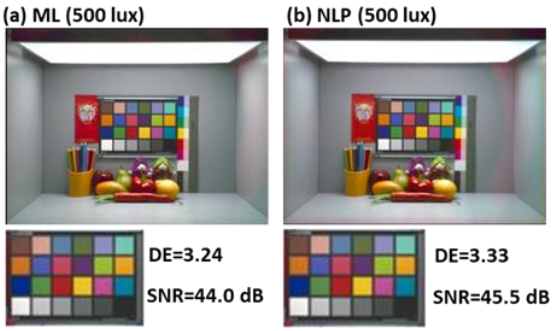


**Fig. 6.** The real images after image signal process at 500 lux condition. (**a**) The ML type image. (**b**) The NLP type image.

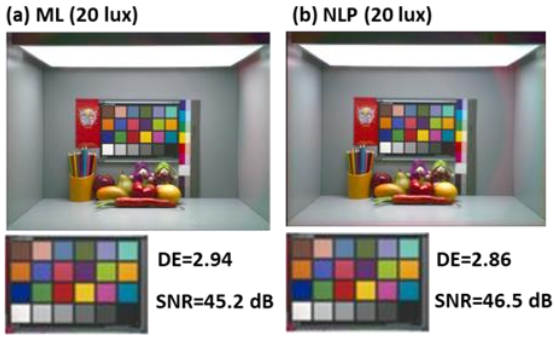


**Fig. 7.** The real images after image signal process at 20 lux condition. (**a**) The ML type image. (**b**) The NLP type image.

Figure 8 shows the measured modulation transfer function (MTF) characteristics of the NLP type image sensor. The MTF curve of the NSP type sensor (blue solid line) is nearly identical to that of the ML type sensor (black solid line) when tested with a module lens of F/# = 2.0. As same as the 0.8 µm single-cell pixel sensor [6], there is no significant difference in MTF between NLP and ML configurations. Furthermore, the same module lens was used for MTF characterization of both the 0.8 µm and 1.6 µm pixel sensors. Based on the clear difference in MTF between the 0.8 µm and 1.6 µm pixel designs, the optical resolution of the module lens is sufficient to distinguish the MTF performance of the NLP and ML types in the 1.6 µm-pixel sensor.

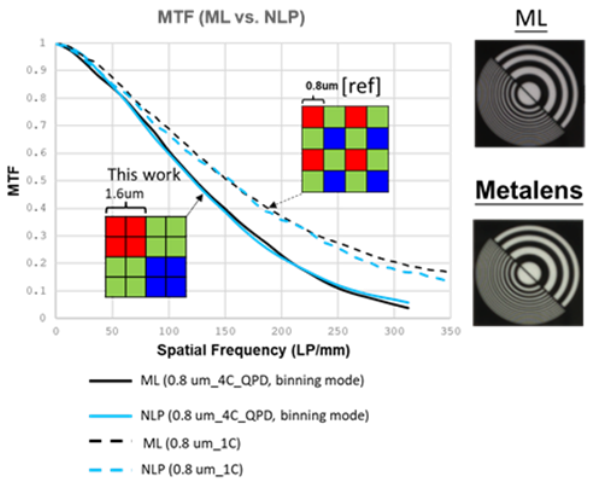


**Fig. 8.** Modulation transfer function measurement based on the same module lens (F/#2.0). Comparison with 1.6 µm (4-cell binning) and 0.8 µm (1-cell) pixel. The 0.8 µm pixel refers to the [ref.6].

## Conclusions

In this work, we successfully demonstrated a double-layer NLP design implemented on a 1.6 µm-pixel CMOS image sensor. The

proposed structure achieved QE enhancements of approximately 11% for the blue channel, 19% for the green channel, and 5% for the red channel. This improvement in QE directly translated into higher signal-to-noise ratio (SNR) performance in real imaging conditions—an increase of +1.5 dB under high illumination (500 lux) and +1.3 dB under low illumination (20 lux)—without degradation in color accuracy or spatial resolution. Furthermore, by optimizing the NLP arrangement near the die edge to match the chief ray angle (CRA) of the module lens, the light-shading characteristics were effectively controlled, exhibiting behavior comparable to that of the conventional ML design. The Gr-Gb signal variation also remained consistent with values reported in previous literature. These results demonstrate that the proposed NLP architecture provides a cost-effective and lithography-compatible solution for enhancing sensitivity in large-pixel CMOS image sensors, particularly for applications such as automotive imaging.

| | ML | NLP |
|---|---|---|
| Quantum efficiency | | B:+11%, G:+19%,R:+5% |
| SNR10 (from QE) | 17.05 | 13.88 (-19%) |
| Color Error | $\Delta E = 3.24$ (@ 500 lux)<br>$\Delta E = 2.94$ (@ 20 $lux$) | $\Delta E = 3.33$ (@ 500 lux)<br>$\Delta E = 2.86$ (@ 20 $lux$) |
| SNR (@500 lux) | | +1.5 dB |
| SNR(@20 lux) | | +1.3 dB |
| Gr-Gb difference | < 2% | 2.3% |
| Resolution | | equivalent |

**Table 1**. Summary table of characteristics of comparison between ML type and NLP type sensor.


## Acknowledgment

This work was supported by Taiwan semiconductor manufacturing company (TSMC).


## References


[1] J. Berzins, S. Fasold, T. pertsch, S. M. B. Baumer, and F. Setzpfandt, "Submicrometer nanostructure-based RGB filters for CMOS image sensors," *ACS Photonics,* vol. **6**, issue 4, pp. 1018–1025, **2019**.

[2] D. Lee, J. Gwak, T. Badloe, S. Palomba, and J. Rho, "Metasurfaces-based imaging and applications: from miniaturized optical components to functional imaging platforms," *Nanoscale Adv.*, vol. **2**, pp. 605-625, **2019**.

[3] J. Hong *et al*., "Adaptive Metasurface Microlens Array for Ultra-Wide-Angle CMOS Image Sensors," *Symposium on VLSI Technology and Circuits (VLSI Technology and Circuits)*, Kyoto, Japan, pp. 1-3, **2025**.

[4] Masashi Miyata, Naru Nemoto, Kota Shikama, Fumihide Kobayashi, and Toshikazu Hashimoto, "Full-color-sorting metalenses for high-sensitivity image sensors," *Optica* **8**, 1596-1604, **2021**.

[5] S. Yun et al., "Highly Efficient Color Separation and Focusing in the Sub-micron CMOS Image Sensor," 2021 IEEE International Electron Devices Meeting (IEDM), San Francisco, CA, USA, pp. 30.1.1-30.1.4, **2021**.

[6] C. -Y. Wang et al., "CMOS image sensor with nano light pillars for optical performance enhancement," 2023 International Electron Devices Meeting (IEDM), San Francisco, CA, USA, pp. 1-4, **2023**.

[7] C. Choi et al., "Optical design of dispersive metasurface nano-prism structure for high sensitivity CMOS image sensor," 2023 International Electron Devices Meeting (IEDM), San Francisco, CA, USA, pp. 1-4, **2023**.

[8] C. Kim et al. "Freeform metasurface color router for deep submicron pixel image sensors". Sci. Adv. **10**, eadn9000, **2024.**

# JOIN US AT THE NEXT EI!

# electronic IMAGING

*Imaging across applications . . . Where industry and academia meet!*

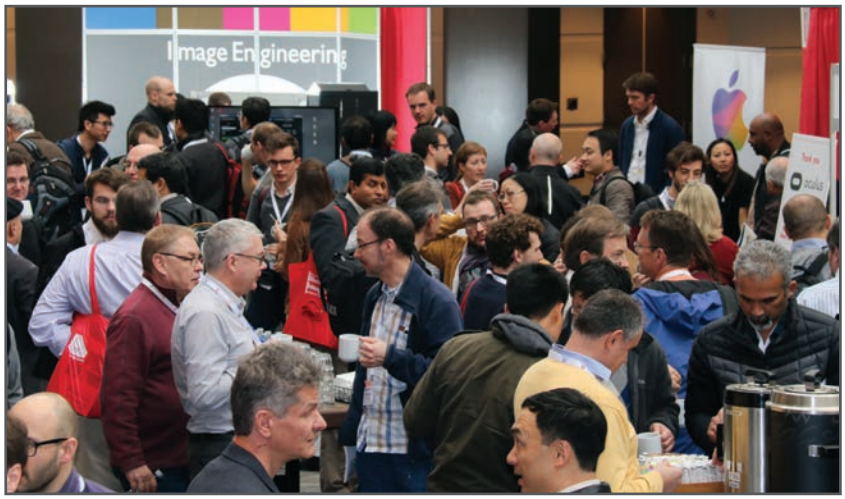



**• SHORT COURSES • EXHIBITS • DEMONSTRATION SESSION • PLENARY TALKS •**
**• INTERACTIVE PAPER SESSION • SPECIAL EVENTS • TECHNICAL SESSIONS •**

## www.electronicimaging.org

ADVANCING IMAGING SCIENCE 75 1947 IS&T 2022 imaging.org